Effect of ZnS shell formation on the confined energy levels of ZnSe quantum dots

Amit D. Lad and Shailaja Mahamuni*
Department of Physics, University of Pune, Pune-411007, India
(Received 28 April 2008; revised manuscript received 1 July 2008; published 29 September 2008)

Photoluminescence excitation spectroscopy was employed to investigate the electronic structure of ZnSe/ZnS core/shell quantum dots. Four excited states *viz.* $1S^e-1S^h_{3/2}$, $1S^e-2S^h_{3/2}$, $1P^e-1P^h_{3/2}$, and $1S^e-1S^{SO}$ are observed in ZnSe and ZnSe/ZnS core/shell quantum dots. The experimentally observed excited states for ZnSe/ZnS quantum dots are analyzed on the basis of reported "effective mass approximation" calculations. The photoluminescence quantum efficiency increased from 2% for ZnSe quantum dots to 42% for ZnSe/ZnS quantum dots. X-ray photoelectron spectroscopic and transmission electron microscopic investigations suggest formation of uniform ZnS shell on ZnSe. The electron energy levels of ZnSe/ZnS core/shell quantum dots are investigated as a function of core diameter and ZnS shell thickness, and are compared with bare ZnSe quantum dots. Seven different sizes (ranging between 20 to 52 Å) are probed using size-selective photoluminescence excitation technique. Upon building a shell of ZnS on ZnSe quantum dots, the transition from three hole states ($1S^h_{3/2}$, $2S^h_{3/2}$, $1S^{SO}$) to $1S^e$ remain well defined and have negligible relative shift, suggesting that the valence-band offset is larger than the energy of these states. With increasing ZnS shell thickness, an observed increase in the transition probability of $1S^e-2S^h_{3/2}$ state is due to modification of hole states caused by ZnS shell. The relative shift of the *P* exciton peak ($1P^e-1P^h_{3/2}$) with increase in shell thickness is due to a loss of confinement energy of *P* electron state. The energy of $1P^e-1P^h_{3/2}$ is found to be remarkably independent as a function of core diameter.

DOI: 10.1103/PhysRevB.78.125421 PACS number(s): 78.67.Hc, 78.55.Et, 73.21.La

I. INTRODUCTION

Colloidal II–VI core/shell semiconductor quantum dots serve as useful fluorescent labels owing to their high photostability, good luminescence efficiency, high oscillator strength, and large emission tunability. Quantum dots have very high surface to volume ratio, which suggests that surface plays a vital role in deciding their electronic and optical properties.[1] Organic cappants are used to passivate the nanocrystalline surface, but effective passivation of anionic, as well as cationic surface sites, is not accomplished by these organic ligands. Epitaxial growth of inorganic semiconductor (shell) on quantum dots (core) can passivate both cationic and anionic dangling bonds and provide better electronic and chemical surface passivation. Depending on the energy gap and the relative position of electron energy levels of the involved semiconductors, the shell can have different functions in core/shell quantum dots.[2] Extensive research is focused toward the type-I core/shell quantum dots for which a shell of higher energy gap material is coated on the narrower energy gap core material.[2–20] Type-I nanoheterostructures typically provide an order-of-magnitude enhancement in PL quantum efficiency. The improvement in PL quantum efficiency is due to proper passivation of surface dangling bonds and nonradiative recombination sites, as well as improved confinement of electrons and holes to the particle core. Charge carrier wave function engineering leads to not only enhanced luminescence quantum efficiency but also useful in carrier separation to minimize the interaction effects and allows an extension of the range of spectral tunability.

Large number of preparative techniques were developed to obtain CdSe-based quantum structures[2,14,15,17–20] with remarkable control on size, shape, and size dispersion along with band offset. Studies on band offset can be carried out on colloidal nanocrystal dispersion. The preparative routes for obtaining high-quality zinc chalcogenide nanoheterostructures are in their infancy. Consequently, further studies on wave function engineering are scarce. ZnSe is a promising material for ultraviolet (UV)–blue light emitting diodes and lasers. ZnSe/ZnS core/shell quantum dots can satisfy the need of current trend of safe handling nanotechnology.[3] The knowledge of electron energy structure along with tunable emission and brightness will make ZnSe/ZnS quantum dots a potential candidate for fabrication of various optoelectronic devices. ZnSe is nontoxic and environmental friendly material. These quantum dots can be useful for biological imaging, DNA analysis, and clinical and therapeutic diagnostics.[21] Along with the linear optical characteristics, the significant nonlinear optical absorption[4,5] exhibit the importance of ZnSe/ZnS quantum dots for fabrication of ultrafast switching and optical limiting devices in a broad spectral region near infrared. Optoelectronic properties of ZnSe/ZnS quantum dots[3–11] have been comparatively less explored, whereas an extensive research was focused toward CdSe/CdS (Refs. 13–18) and CdSe/ZnS (Refs. 2 and 18–20) quantum dots. The natural band alignment for ZnSe/ZnS system indicates a type-I character, with a valence-band offset of 0.55 eV and conduction-band offset of 0.33 eV.[22] The synthesis of ZnSe/ZnS core/shell quantum dots is state of the art and to date very few reports have arrived.[3–11] Various core/shell quantum dots such as CdSe/CdS (Refs. 13–18) and CdSe/ZnS (Refs. 2 and 18–20) exhibit the photoluminescence (PL) quantum efficiency more than 30%. ZnSe/ZnS nanocrystals, having mixed phase (namely, zinc-blende and wurtzite) crystalline core, indicated 2.6-fold enhancement in PL intensity.[9] ZnSe/ZnS core/shell nanocrystals studied earlier show the PL quantum efficiency of 17% (Ref. 7) to 32% (Ref. 8). Time-resolved transient absorption measurements[3] of ZnSe/ZnS core/shell nanoparticles exhibited the confinement of hole to

ZnSe core. The electronic structure of core/shell quantum dots is found to be governed by the band alignment,[13,16,17,19] strain effect,[16] and quantum confinement.[2,13,16,17,19] Hence, the knowledge of electronic structure of ZnSe/ZnS core/shell quantum dots is the prime step in futuristic device-oriented applications. The band offsets between ZnSe/ZnS nanoheterostructure components are determining parameters for their optoelectronic properties, for example, the degree of charge-carrier separation, localization, and hence the excited state dynamics. Due to lack of direct experimental measurements, a common approach taken in this context so far is to assume band offset values of the bulk materials.

In the present study, high-temperature wet chemical route has been adopted to synthesize ZnSe and ZnSe/ZnS quantum dots. ZnSe quantum dots are coated with a varying ZnS shell thickness and are thoroughly investigated by means of photoluminescence spectroscopy. The size-selective photoluminescence excitation (PLE) spectroscopy is employed to map the electronic structure of ZnSe and ZnSe/ZnS quantum dots. Electron energy levels of ZnSe/ZnS core/shell quantum dots were studied and compared with that of bare ZnSe quantum dots. Four excited states in ZnSe/ZnS quantum dots were observed. The effect of shell thickness on the electron energy levels of ZnSe quantum dots is discussed. This is a comprehensive report on the electronic structures of ZnSe/ZnS core/shell quantum dots as a function of the core size as well as shell thickness.

II. EXPERIMENTAL DETAILS

ZnSe quantum dots have been synthesized according to the method described by Hines and Guyot-Sionnest (Ref. 23) and modified by the method described by Peng *et al.*[24] to achieve the different sizes. In typical synthesis,[25] appropriate amounts of diethylzinc ($ZnEt_2$) and trioctylphosphine (TOP) selenide were injected in hot 1-hexadecylamine. ZnSe quantum dots were collected in the powder form and redispersed in hexane.

For ZnS coating $ZnEt_2$ and hexamethyldisilathiane in TOP were used as the Zn and S source, respectively. The ZnS shell was grown on ZnSe quantum dots according to the method similar to that of CdSe/ZnS quantum dots described by Dabbousi *et al.*[19] Here we assume one monolayer ZnS shell measures 2 Å along the radius of spherical ZnSe quantum dots. In the present study, up to four monolayers of ZnS shell has been overcoated on ZnSe quantum dots. The core/shell nanocrystals were isolated from the reaction solution, washed several times with *n*-butanol and methanol, dried in vacuum, and dispersed in hexane for various characterizations.

X-ray diffraction (XRD) measurements were carried out on Bruker AXS D8 advance powder x-ray diffractometer, using Cu K_α ($\lambda = 1.5402$ Å) as an incident radiation. The average size of quantum dots is estimated using Scherrer formula by considering the line broadening of the XRD patterns.[26] Transmission electron microscopic (TEM) measurements were carried out using a Philips CM200 microscope operating at 200 kV.

X-ray photoelectron spectroscopic (XPS) measurements were carried out on an electron spectrometer from VSW Scientific Instruments Ltd., U. K. The base pressure of the spectrometer was about 3×10^{-9} mbar. Experiments were performed using Al K_α radiation at analyzer pass energy of 40 eV. The typical resolution of the spectrometer is approximately 0.9 eV.

Optical absorption measurements were carried out on JASCO V-670 spectrophotometer. The PL emission and PLE measurements were carried out on Perkin Elmer LS 55 fluorescence spectrometer. Fluorescence spectrometer consists of pulsed xenon lamp (7.3 W average power at 50 Hz), holographic grating excitation and emission monochromators, and well plate reader. The PL quantum efficiency of ZnSe, as well as ZnSe/ZnS quantum dots in hexane, was estimated relative to stilbene 420 in methanol of the same concentration.

The inhomogeneous broadening of the spectral features is unavoidable due to the finite size and shape distribution. PLE can be used to select the optical window in order to examine the absorption of narrow size distributed quantum dots.[25,27] In PLE, a spectrally narrow portion of the emission is monitored, while the excitation energy is scanned. The spectrum of the emission amplitude as a function of the excitation energy provides an absorption spectrum for the subset of the particles which emit at the monitored wavelength. Thus PLE can be used as a size-selective optical technique. The PLE data obtained by fixing the emission on the blue edge of the luminescence peak at different wavelengths with an interval of 10 nm correspond to sizes ranging from 20 to 52 Å. In PLE, when excitation wavelength approaches the emission wavelength, excitation features are superimposed on the exponential increasing background. When excitation and emission wavelengths match exactly, one can observe large increase in background intensity and is known as the fundamental diffraction peak of the grating. All PLE spectra are corrected for an exponentially increasing background function to eliminate the effect of the fundamental diffraction peak of the grating.

III. RESULTS AND DISCUSSION

A. Structural characterization

The crystalline phase and average size of quantum dots was determined by XRD. Three different-sized ZnSe quantum dots (*viz.* ZnSe-I: 45 Å ± 13%, ZnSe-II: 35 Å ± 11%, and ZnSe-III: 25 Å ± 16%) were synthesized and overcoated by ZnS shell up to four monolayers. The XRD patterns of ZnSe/ZnS quantum dots show broad peaks corresponding to (1 1 1), (2 2 0), and (3 1 1) planes of cubic zinc-blende phase of ZnSe, suggesting that the diffraction is predominantly due to ZnSe core. With increase in ZnS thickness, the peak width remains constant while the position of diffraction features shift toward higher (ZnS) values as shown in Fig. 1. The distribution of bond lengths resulting from the strain is responsible for maintaining the XRD peak width constant,[14] though there is an increase in the quantum dot diameter due to the shell growth. Absence of peak narrowing with increasing ZnS thickness also rules out the possibility of alloy formation. The lattice mismatch between ZnSe and ZnS is about 4.2% giving the lattice strain throughout the nanohetero-

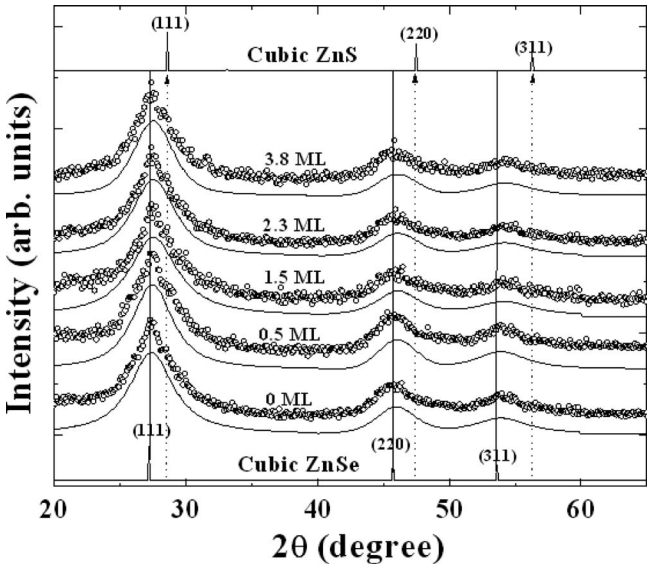

FIG. 1. XRD pattern of ZnSe-I quantum dots with varying monolayers (ML) of ZnS shell thickness. Symbols represent the experimental data, whereas the solid line is the Gaussian fit to the experimental data.

structure. ZnSe near the interface experiences a net compressive strain, while ZnS experiences a net expansive strain. This leads to a consistent increase in the average lattice constants throughout the shell growth. Strain modifies the band alignment of core/shell structures. It modifies band offset and is responsible for increase in energy gap of core/shell quantum dots.[16] Hence, the presence of strain can alter the electron energy levels.[16]

The thickness of ZnS shell, crystal structure, and shape of ZnSe/ZnS core/shell quantum dots is precisely determined by TEM. Figure 2 shows TEM images of ZnSe/ZnS-I core/shell quantum dots with different monolayers of ZnS shell thickness. The spherical shape is retained by core/shell quantum dots. TEM indicates the size 48 Å ± 10%, 52 Å ± 9%, 55 Å ± 11%, and 61 Å ± 13% for 0.5, 1.5, 2.3, and 3.8 monolayers of ZnSe/ZnS-I core/shell quantum dots, respec-

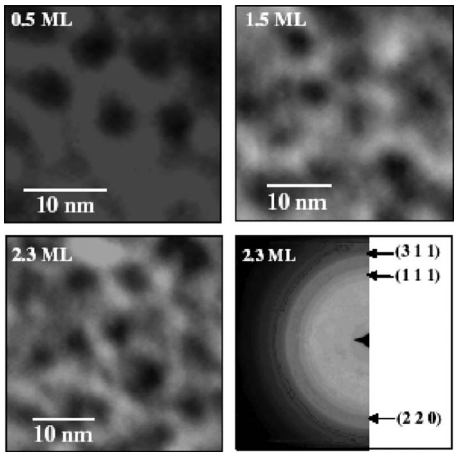

FIG. 2. TEM images of ZnSe/ZnS-I core/shell quantum dots with 0.5, 1.5, and 2.3 monolayers (ML) ZnS thickness; and electron diffraction pattern of ZnSe/ZnS-I: 2.3 ML quantum dots.

TABLE I. Diameter measured by TEM, thickness of shell determined by TEM as well as by XPS measurements, and intensity ratio of S $2p_{3/2}$ to Se $3p_{3/2}$ obtained by XPS analysis for different building of ZnS shell over ZnSe-I quantum dots.

ZnSe/ZnS-I	Diameter by TEM (Å)	Thickness of shell (Å) by TEM	by XPS	I(S $2p_{3/2}$) / I(Se $3p_{3/2}$)
0.0	46 ± 11%			
0.5	48 ± 10%	1.0	1.4	1.42
1.5	52 ± 9%	3.0	3.2	3.19
2.3	55 ± 11%	4.5	4.1	4.08
3.8	61 ± 13%	7.5	7.0	6.95

tively (Table I). The size of ZnSe-I core quantum dots is found to be 46 Å ± 11%.[4,5,25] Estimation of the shell thickness in the case of ZnSe/ZnS-I quantum dots helped to optimize the synthesis procedure for ZnSe/ZnS-II and ZnSe/ZnS-III quantum dots to keep the constant shell thickness as to that of ZnSe/ZnS-I quantum dots. Electron diffraction pattern of core/shell quantum dots shows the diffraction rings corresponding to (1 1 1), (2 2 0), and (3 1 1) lattice planes of zinc-blende phase of ZnSe exclusively. The consistent decrease in interplanar distance is observed with increase in ZnS shell thickness. This observation is also consistent with the XRD data.

XPS measurements (Fig. 3) were carried out on ZnSe/ZnS core/shell quantum dots. Survey spectra (not shown here) show presence of Zn, Se, and S species along with C and O. The presence of C and O is mostly due to the atmospheric contamination. The position of C 1s line at 284.6 eV indicates the absence of significant charging. The Se 3p spec-

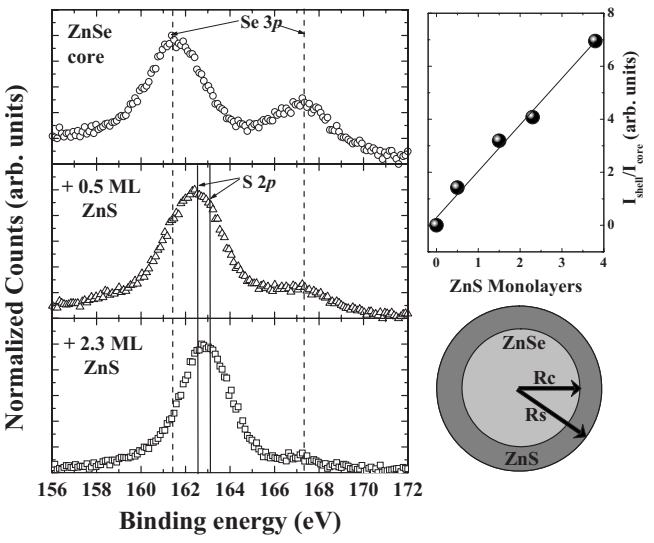

FIG. 3. (Left) XPS spectra of bare ZnSe-I core and ZnSe/ZnS-I core/shell quantum dots. (Right) Intensity ratio of S $2p_{3/2}$ to Se $3p_{3/2}$ of peaks with respect to shell thickness. Schematic representation of ZnSe/ZnS core/shell quantum dot structure used for XPS analysis. R_c is the radius of core, whereas R_s is the radius of core/shell quantum dot.

trum exhibits a spin-orbit doublet structure corresponding to $3p_{3/2}$ and $3p_{1/2}$ signals with binding energy 161.5 and 167.3 eV, respectively. The spin-orbit doublet of S $2p$ level splits into $2p_{3/2}$ and $2p_{1/2}$ with binding energy 162.4 and 163.3 eV, respectively. The gradual decrease in the intensity of Se $3p$ peak and an increase in the intensity of S $2p$ peak are observed as the shell thickness increases from 0 to 3.8 monolayers, thus indicating a uniform coating[15] of ZnSe with ZnS shells.

To calculate the thickness of the shell using XPS investigations, we have used the method suggested by Nanda and Sarma.[28] The intensity ratio of the shell to core can be expressed as[28]

$$\frac{I_{\text{shell}}}{I_{\text{core}}} = \frac{I_0^{\text{ZnS}}}{I_0^{\text{ZnSe}}} \frac{\int_{R_c}^{R_s} \int_0^{\pi} \exp\left[\frac{-f(r,\theta)}{\lambda}\right] r^2 dr \sin\theta \, d\theta}{\int_0^{R_c} \int_0^{\pi} \exp\left[\frac{-f(r,\theta)}{\lambda}\right] r^2 dr \sin\theta \, d\theta}, \quad (1)$$

where, $f(r,\theta)=(R^2-r^2\sin^2\theta)^{1/2}-r\cos\theta$; λ is the mean free path of photoionized electrons (21 Å in case of Se $3p$ and S $2p$ levels); $I_0^{\text{ZnS}}/I_0^{\text{ZnSe}}=(\rho^{\text{ZnS}}/M^{\text{ZnS}})(M^{\text{ZnSe}}/\rho^{\text{ZnSe}})=1.12$; ρ^{ZnS} and ρ^{ZnSe} are the densities and M^{ZnS} and M^{ZnSe} are molecular weights of ZnS and ZnSe, respectively. The intensity ratio of S $2p_{1/2}$ to Se $3p_{1/2}$ (Table I) has been considered for the evaluation of Eq. (1). The schematic representation of ZnSe/ZnS core/shell quantum dots is shown in Fig. 3. R_c represents the radius of core, whereas R_s represents the radius of core/shell quantum dot. The above integrals were computed numerically for varying choices of core/shell radius (R_s). The limits for the integration of the core were kept constant [23 Å for ZnSe-I quantum dots (R_c), as determined from TEM]. To calculate the thickness of the shell the values of R_s were varied so that calculated intensity ratio [from Eq. (1)] matched the ratio with the experiment (Table I). The shell thickness calculated by the XPS spectra agrees well with the TEM investigations (Table I).

B. Influence of ZnS shell on confined energy levels of ZnSe quantum dots

1. Optical absorption investigations

The optical absorption of ZnSe-I, ZnSe-II, and ZnSe-III is found to be at 410 nm (3.02 eV), 382 nm (3.25 eV), and 364 nm (3.41 eV), corresponding to the sizes estimated from the tight-binding calculations[29] to be 43, 33, and 24 Å, respectively. The bulk Bohr exciton diameter of ZnSe is 90 Å,[30] suggesting that all quantum dots studied here are in the strong confinement regime. The fitting of optical absorption spectrum was performed to identify various higher excited states in ZnSe and ZnSe/ZnS quantum dots.[7] Three excited states are seen in the optical absorption spectra (Fig. 4). These transitions are assigned to $1S^e-1S^h_{3/2}$, $1S^e-2S^h_{3/2}$, and $1P^e-1P^h_{3/2}$, as designated in effective mass approximation (EMA) formalism.[1,31,32] The optical absorption spectra of ZnSe/ZnS quantum dots reveal the constant area under the lowest excitonic transition $1S^e-1S^h_{3/2}$, indicative of constant oscillator strength[19] for varying ZnS shell thickness (Fig. 4).

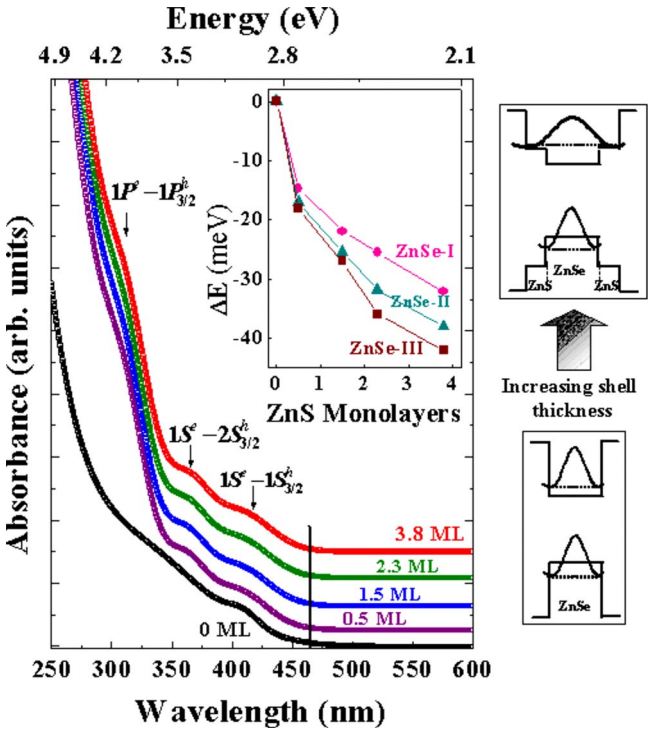

FIG. 4. (Color online) (Left) Optical absorption spectra of ZnSe/ZnS-I core/shell quantum dots. Various higher excited states are indicated. All optical absorption spectra are normalized with respect to $1S^e-1S^h_{3/2}$ transition, and are shifted upward [by 0.1, 0.3, 0.5, and 0.8 for 0.5, 1.5, 2.3, and 3.8 monolayers (ML), respectively] for the clarity. The solid line indicates the energy gap of bulk ZnSe. The inset indicates the observed redshift (ΔE) in the $1S^e-1S^h_{3/2}$ transition of three different-sized core/shell quantum dots with respect to its corresponding core quantum dots. (Right) Schematic energetics for ZnSe and ZnSe/ZnS core/shell structures.

With increase in ZnS shell thickness, the redshift in $1S^e-1S^h_{3/2}$ transition is observed (Fig. 4). Inset of Fig. 4 shows the redshift in the absorption spectra as a function of core size of quantum dots. The larger redshift in smaller quantum dots is due to large spreading of electron wave function into ZnS shell. This effect is also attributed to relaxation of quantum confinement resulting from the growth of the shell.[12,18] A contribution to the redshift in the case of ZnSe/ZnS quantum dots could be partially due to the strain at the core/shell interface.[7] Strain modifies the band alignment of core/shell structure. Li and Wang[16] proved that strain changes the band offset and hence the wave functions and energy eigenvalues. In type-I quantum dots, the core experiences a net compressive strain near the interface, while the shell experiences a net expansive strain. This results in increase in the energy gap of quantum dots, and will be reflected from blueshift in the optical absorption spectra. The absence of blueshift in the absorption spectra indicates that strain is not playing the important role[7] in the present case.

2. Photoluminescence investigations

The PL emission maximum at room temperature for ZnSe-I, ZnSe-II, and ZnSe-III quantum dots is observed at 420 nm (2.95 eV), 408 nm (3.04 eV), and 400 nm (3.10 eV),

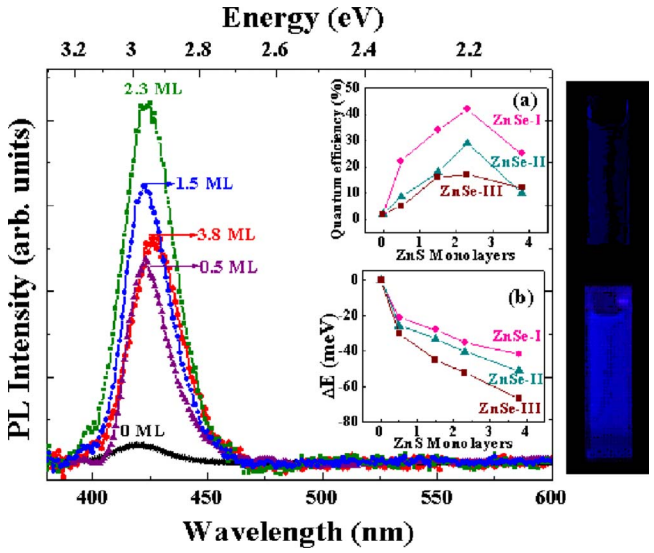

FIG. 5. (Color online) (Left) PL spectra for ZnSe-I quantum dots for varying thickness of ZnS shell. Inset shows (a) PL quantum efficiency variation for three different-sized core/shell quantum dots; (b) the observed redshift in the PL emission energy (ΔE) of the core/shell quantum dots with respect to its corresponding core quantum dots. (Right) Fluorescence of ZnSe-I quantum dots with ZnS shell thickness of 0 monolayer (top) and 2.3 monolayers (bottom) excited with UV light.

respectively. ZnSe quantum dots exhibit only band-edge luminescence. The observed size-dependent Stokes shift is discussed elsewhere.[25] PL spectra of ZnSe-I quantum dots with varying thickness of ZnS shell are presented in Fig. 5. The narrow photoluminescence [full width at half maximum (FWHM) $\leq$30 nm] from the core/shell quantum dots spans the spectrum from UV through blue. PL FWHM of core/shell quantum dots is within the experimental error of ZnSe cores. This demonstrates the good control on size distribution of the core/shell quantum dots. Inset of Fig. 5 shows the increase in PL quantum efficiency with shell thickness for three series of ZnSe/ZnS core/shell quantum dots. The PL quantum efficiency is increased dramatically from 2 to 42%. ZnSe/ZnS core/shell nanocrystals studied earlier also showed around twenty times enhancement in PL quantum efficiency as compared to corresponding core nanocrystals.[11] In the case of core ZnSe quantum dots the charge carriers are delocalized throughout the quantum dot. Whereas in ZnSe/ZnS core/shell quantum dots, the strong valence-band offset confines hole to the core and enhances quantum efficiency, while the small conduction-band offset ensures spectral tunability by the reduction of confinement energy of electron. In case of CdSe/CdS core/shell structures,[22] the conduction-band offset is 0.27 eV, whereas the valence-band offset is 0.51 eV. In this type of quantum dots, it is shown that the electron is delocalized throughout the core/shell structure while the hole is perfectly confined to CdSe core.[14] The present results are in excellent agreement with CdSe/CdS quantum dots. Recent time-resolved transient absorption measurements[3] of ZnSe/ZnS core/shell nanoparticles also indicated the confinement of hole to ZnSe core. The hole is confined in quantum dot due to the built-in nanostructure potential while the electron is confined only due to the Coulomb interaction with the hole.[17,33] The electron wave function is distributed over a core/shell region, and the hole wave function is strongly confined inside a core. The strong hole confinement in ZnSe/ZnS causes core/shell system to have the large electron-hole Coulomb interaction. First-principles investigations[16] also exhibit large electron-hole Coulomb interaction in CdSe/CdS core/shell quantum dots due to strong hole confinement. The localization of hole wave function in ZnSe core is a prime factor responsible for increase in the PL quantum efficiency,[3,6] and hence it cannot be involved in oxidation degradation processes.[2] The consistent increase in the PL quantum efficiency up to 2.3 monolayers of ZnSe/ZnS quantum dots is observed (inset of Fig. 5). The maximum PL quantum efficiency value at 2.3-monolayer-thick ZnS shell implies the proper passivation of surface dangling bonds and nonradiative recombination sites. The reduction in the PL quantum efficiency is observed as shell thickness is increased further (>2.3 monolayers). This decrease in the PL quantum efficiency is tentatively attributed to formation of the defects in ZnS shell.[19] A thicker coating (>2.3 monolayers) can produce stacking faults in the layer due to the lattice mismatch[2] of ZnSe and ZnS. Stacking faults in the layer can create radiationless relaxation, which in turn is responsible for decrease in PL quantum efficiency.[2] With increase in ZnS shell thickness the PL spectra show a consistent redshift (inset of Fig. 5). The redshift in the PL spectra is slightly larger than the shift in the absorption spectra.

3. Size-selective photoluminescence excitation study

Seven different sizes (ranging between 20 to 52 Å) from three subsets of samples were probed using size-selective PLE technique. The PLE spectra are obtained by fixing the emission on the blue edge of PL peak. The size of quantum dots is estimated from first excitonic feature ($1S^e-1S^h_{3/2}$) of the PLE employing reported tight-binding calculations[29] for ZnSe quantum dots. Figure 6 shows PLE spectra of ZnSe/ZnS quantum dots monitored at 3.10 eV. Four higher excited state transitions were observed. These transitions are assigned to $1S^e-1S^h_{3/2}$, $1S^e-2S^h_{3/2}$, $1P^e-1P^h_{3/2}$, and $1S^e-1S^{SO}$, as designated in EMA formalism.[1,31,32]

In quantum dots, where the size of the particles is much larger than the lattice constant of the material, EMA can be used to give a quantitative description of the size-dependent electronic properties. ZnSe/ZnS quantum dots studied here are in the strong confinement regime. Xia[31] has used the spherical quantum well model to simulate the quantum dots and used the effective-mass envelope function method to calculate the electronic structure of ZnSe quantum dots. The effective-mass model is combined with spherical boundary conditions, and the electrons and holes are treated independently.[32] In zinc-blende semiconductor, three distinct valence bands (heavy hole, light hole, and spin-orbit split-off) were considered.[1] The spherical symmetry of the quantum dots introduces an orbital angular momentum that couples with the intrinsic $J=3/2$ momentum of the valence-band Bloch functions. Good quantum number is the total angular momentum, $F=L+J$, where L is the angular momentum of envelope function and J is the valence-band angular

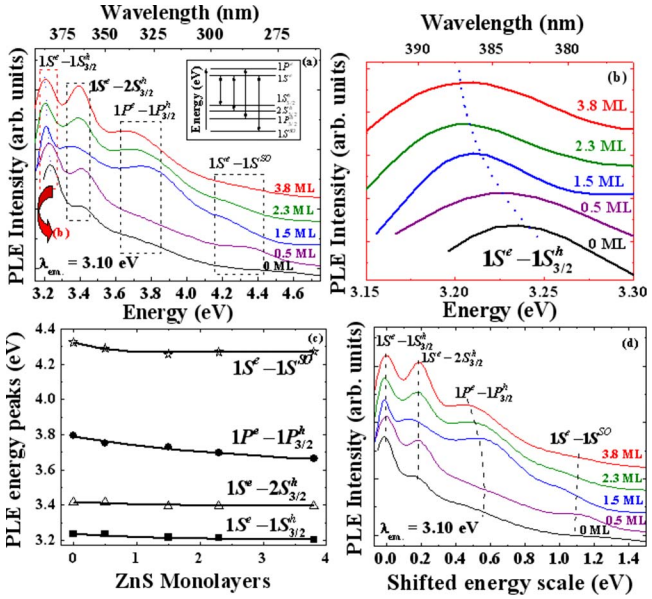

FIG. 6. (Color online) (a) PLE spectra of ZnSe quantum dots with different thickness of ZnS shell, monitored at 3.10 eV (400 nm). All PLE spectra are normalized with respect to $1S^e-1S^h_{3/2}$ transition, and are shifted upward [by 0.1, 0.3, 0.5, and 0.7 for 0.5, 1.5, 2.3, and 3.8 monolayers (ML), respectively] for the clarity. Inset exhibits the schematic of electron energy levels in ZnSe and ZnSe/ZnS quantum dots. (b) The enlarged portion of PLE spectra exhibiting only $1S^e-1S^h_{3/2}$ transition. (c) Variation of electron energy levels of ZnSe quantum dots having diameter 33 Å as a function of shell thickness. Energies are extracted from PLE spectra (a). (d) The PLE spectra [shown in (a)] are shifted by energy of $1S^e-1S^h_{3/2}$ transition.

momentum. As a result, the hole wave functions contain linear combinations of L and $L+2$ envelope functions. F is the good quantum number for valence states of the cubic semiconductor with $J=3/2$ for light-hole and heavy-hole bands, while $J=1/2$ for the spin-orbit split-off band. The electron states are simply given by nL^e, where n is the number of the level in energy ordering. The subscript e implies an electron state. The hole states are given by nL_F. This is a reasonable approach for wide energy gap semiconductor quantum dots such as ZnSe,[25] CdSe,[27] and CdTe.[34] The conduction band of ZnSe has Zn $2s$ character, whereas the valence band has Se $4p$ character.[31] The first excited state transition $1S^e-1S^h_{3/2}$ indicates the electron and hole both in the first S-like envelope function.[1] The transition $1S^e-2S^h_{3/2}$ arises due to S-D mixing.[31,32] The transition $1S^e-1S^{SO}$ involves the spin-orbit split-off hole state.[1,31]

The inset of Fig. 6(a) exhibits the schematic of electron energy levels in ZnSe and ZnSe/ZnS quantum dots. The band-edge transition $1S^e-1S^h_{3/2}$ is observed around 3.25 eV (382 nm) when emission wavelength is monitored at 3.10 eV (400 nm). This is equivalent to probing[29] ZnSe quantum dots of 33 Å in diameter. The first excited state of ZnSe quantum dots with ZnS shell formation is presented for comparison in Fig. 6(b). With increase in shell thickness, the small redshift in the energy of the $1S^e-1S^h_{3/2}$, $1S^e-2S^h_{3/2}$, and $1S^e-1S^{SO}$ transitions is observed [Fig. 6(c)]. On the other hand, the large redshift of around 130 meV in $1P^e-1P^h_{3/2}$ transition is observed with the increase in ZnS monolayer from 0 to 3.8 [Fig. 6(c)].

Xia[31] has shown that the transition probability of $1S^e-1S^h_{3/2}$ state for ZnSe quantum dots is 2.4 times larger than that of the $1S^e-2S^h_{3/2}$ state. Experimental measurements of bare ZnSe quantum dots exhibit the similar trend.[25] The overlap integrals of radial wave functions were found to be[31] 0.833 and 0.543 for $1S^e-1S^h_{3/2}$ and $1S^e-2S^h_{3/2}$ transitions, respectively. As compared to bare ZnSe quantum dots, ZnS shell has its main effects on the valence energy levels. With increasing ZnS shell thickness the increase in the transition probability of $1S^e-2S^h_{3/2}$ state is observed [Fig. 6(a)]. Loss of confinement of S state in case of ZnSe/ZnS quantum dots can alter the S-D mixing and hence the overlap integrals of radial wave functions for $1S^e-1S^h_{3/2}$ and $1S^e-2S^h_{3/2}$ transitions will get modified. This leads to enhancement in the transition probability of $1S^e-2S^h_{3/2}$ state.

These PLE spectra [shown in Fig. 6(a)] are shifted so that the energy of $1S^e-1S^h_{3/2}$ transition becomes 0 meV [Fig. 6(d)]. Upon building a shell of ZnS on ZnSe, the transition from three hole states ($1S^h_{3/2}$, $2S^h_{3/2}$, $1S^{SO}$) to $1S^e$ remain well defined and have negligible relative shift, suggesting that the valence-band offset is larger than the energy of these states. Whereas, small conduction-band offset allows electron wave function to penetrate into ZnS shell, and is responsible for loss of confinement of S as well as P states. The relative shift of the P exciton peak ($1P^e-1P^h_{3/2}$) is indicative of the loss in the confinement energy of P electron state. The loss of confinement of P electron states is greater than loss of confinement of S electron and hence is responsible for the relative shift of the P ($1P^e-1P^h_{3/2}$) exciton peak. Similar effect is also observed in type-I zinc-blende CdSe/CdS quantum dots.[13] Also, the energies of the hole states are seen to be remarkably independent of the shell thickness. Electronic structure of CdSe/CdS nanocrystals was calculated with the help of EMA.[17] For the CdSe/CdS nanocrystals,[17] the electron energy shift was found to be reduced with an increase in shell thickness due to the spreading electron density distribution. However, the hole energy shift was found to be significantly unaltered because of the localization of holes in the CdSe core.[17] The present investigations reveal analogous trend.

Figure 7 shows the transitions from different excited states with varying ZnS shell thickness for all different-sized ZnSe/ZnS core/shell quantum dots. The solid lines in Fig. 7 serve as a visual guide for the various transitions. The energies are extracted from the PLE data. The redshift in the energy of $1S^e-1S^h_{3/2}$, $1S^e-2S^h_{3/2}$, $1P^e-1P^h_{3/2}$, and $1S^e-1S^{SO}$ transitions is clearly observed with an increase in ZnSe core diameter. The redshift is a result of decrease in kinetic energy of the excited electron and hole due to spreading of their wave functions in the shell. The redshift is more pronounced in smaller quantum dots due to spreading of electron wave function into shell and is dominated by the confinement energies of the charge carriers.

The variation in energy of the excited state transitions with respect to the energy of the first excited state ($1S^e-1S^h_{3/2}$) is displayed in Fig. 8. The solid lines in Fig. 8 serve as a visual guide for the various transitions. Figure 8 indi-

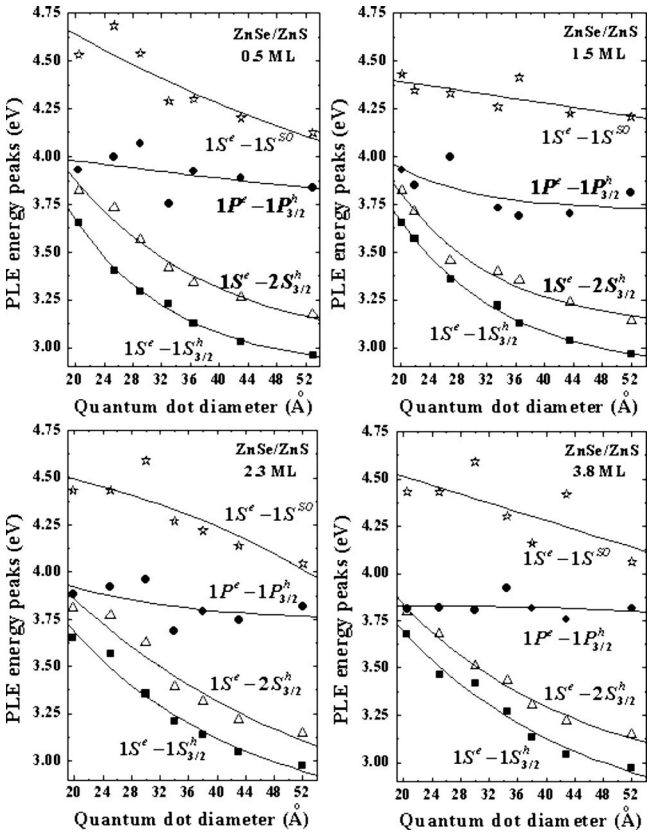

FIG. 7. PLE energies for various transition states as function of quantum dot diameter of ZnSe/ZnS core/shell quantum dots. The solid lines serve as visual guide for the transitions.

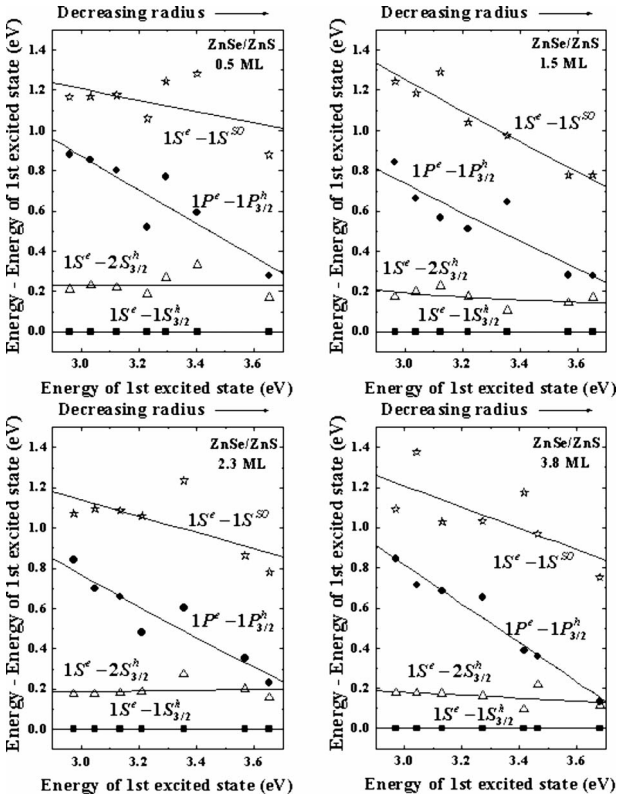

FIG. 8. Transition energies versus energy of the first excited state. The transition energies have been probed by the PLE spectroscopy. The solid lines serve as visual guide for the transitions.

cates the relative shift in the excited state transitions. Each section of Fig. 8 is representative of electronic energy levels for fixed ZnS shell thickness but varying ZnSe core radius. The *x*-axis label, energy of fist excited state, is a strongly size-dependent parameter. The energy of $1S^e-2S^h_{3/2}$ transition is found to be remarkably independent of core radius. Relative redshift in the energy of $1P^e-1P^h_{3/2}$ and $1S^e-1S^{SO}$ transitions are observed with decrease in core radius. As described earlier, loss of confinement of *S* and *P* states of ZnSe quantum dots is expected due to the formation of shell growth. Effects of finite spin-orbit splitting (Δ) on optical properties of spherical semiconductor quantum dots are thoroughly discussed by Richard *et al.*[34] A significant influence of the spin-orbit split-off band is found in cases where spin-orbit splitting is large, like for ZnSe (Δ=430 meV).[31] The spin-orbit split-off band has a substantial influence on the optical properties of spherical semiconductor crystallites.[34] The relative position of $1S^e-1S^{SO}$ is mostly dependent on spin-orbit split-off energy. In the present case, relative shift of $1S^e-1S^{SO}$ transition is found to be complicated as a function of ZnSe core diameter. The first-principles calculation will be extremely helpful in this regard. We are trying to calculate the energy levels of ZnSe quantum dots as a function of core diameter and ZnS shell thickness by *ab initio* pseudopotential approach. It will form a topic of the future publication.

IV. CONCLUSIONS

Two-step high-temperature wet chemical route was adopted to produce highly luminescent ZnSe/ZnS core/shell quantum dots. The present study probes effect of ZnS shell formation on electronic energy levels of ZnSe quantum dots. Three different-sized ZnSe quantum dots were overcoated by varying thickness of ZnS shell. The formation of shell on ZnSe quantum dots is evident from absorption, PL, PLE, XRD, TEM, and XPS measurements. The absence of blueshift in the absorption spectra indicates that strain is not playing the important role in the present case. The narrow PL of core/shell quantum dots spans the spectrum from UV through blue with quantum efficiency of 5 to 42% at room temperature. Seven different sizes (ranging between 20 to 52 Å) from three subsets of samples were probed using size-selective PLE technique. With increase in shell thickness of ZnS on ZnSe quantum dots, the transition from three hole states ($1S^h_{3/2}$, $2S^h_{3/2}$, $1S^{SO}$) to $1S^e$ remain well defined and have negligible relative shift, suggesting that the valence-band offset is larger than the energy of these states. Moreover, the increase in the transition probability of $1S^e-2S^h_{3/2}$ state is also observed. The relative shift of the *P* exciton peak is due to a loss of confinement energy of *P* electron state. The energies of the hole states are seen to be remarkably independent of the shell thickness. The knowledge of ZnS shell formation on the electron energy levels of ZnSe quantum dots will be instructive in the fabrication of various optoelectronic devices.

ACKNOWLEDGMENTS

The authors are thankful to the Department of Science and Technology (DST) for financial support. The authors would like to acknowledge the DST Unit on Nanoscience for PL, C.N.Q.S. for XRD, and S.A.I.F. I.I.T. Mumbai for the TEM facility. The authors thank T. Shripathi and U. P. Deshpande for the use of XPS at UGC-DAE Consortium for Scientific Research, Indore. The authors are thankful to Ch. Rajesh and Shweta Patankar for help in the experiments.

*shailajamahamuni@yahoo.co.in

[1] U. Woggon, *Optical Properties of Semiconductor Quantum Dots* (Springer, Berlin, 1997).
[2] A. Eychmuller, J. Phys. Chem. B **104**, 6514 (2000).
[3] V. V. Matylitsky, A. Shavel, N. Gaponik, A. Eychmuller, and J. Wachtveitl, J. Phys. Chem. C **112**, 2703 (2008).
[4] A. D. Lad, P. P. Kiran, G. R. Kumar, and S. Mahamuni, Appl. Phys. Lett. **90**, 133113 (2007).
[5] A. D. Lad, P. P. Kiran, D. More, G. R. Kumar, and S. Mahamuni, Appl. Phys. Lett. **92**, 043126 (2008).
[6] V. V. Nikesh and S. Mahamuni, Semicond. Sci. Technol. **16**, 687 (2001).
[7] M. Lomascolo, A. Creti, G. Leo, L. Vasanelli, and L. Manna, Appl. Phys. Lett. **82**, 418 (2003).
[8] H.-S. Chen, B. Lo, J.-Y. Hwang, G.-Y. Chang, C.-M. Chen, S.-J. Tasi, and S.-J. Jassy Wang, J. Phys. Chem. B **108**, 17119 (2004).
[9] M. Ali and D. D. Sarma, J. Nanosci. Nanotechnol. **7**, 1960 (2007).
[10] Y. G. Kim, Y. S. Joh, J. H. Song, K. S. Baek, S. K. Chang, and E. D. Sim, Appl. Phys. Lett. **83**, 2356 (2003).
[11] K.-K. Song and S. Lee, Curr. Appl. Phys. **1**, 169 (2001).
[12] M. Danek, K. F. Jensen, C. B. Murray, and M. G. Bawendi, Chem. Mater. **8**, 173 (1996).
[13] A. Pandey and P. Guyot-Sionnest, J. Chem. Phys. **127**, 104710 (2007).
[14] X. Peng, M. C. Schlamp, A. V. Kadavanich, and A. P. Alivisatos, J. Am. Chem. Soc. **119**, 7019 (1997).
[15] J. J. Li, Y. A. Wang, W. Guo, J. C. Keay, T. D. Mishima, M. B. Johnson, and X. Peng, J. Am. Chem. Soc. **125**, 12567 (2003).
[16] J. Li and L.-W. Wang, Appl. Phys. Lett. **84**, 3648 (2004).
[17] C. L. Weng, I. Chuen Chen, and Y. C. Tsai, Phys. Rev. B **76**, 195313 (2007).
[18] M. A. Malik, P. O'Brien, and N. Revaprasadu, Chem. Mater. **14**, 2004 (2002).
[19] B. O. Dabbousi, J. Rodriguez-Viejo, F. V. Mikulec, J. R. Heine, H. Mattoussi, R. Ober, K. F. Jensen, and M. G. Bawendi, J. Phys. Chem. B **101**, 9463 (1997).
[20] D. V. Talapin, A. L. Rogach, A. Kornowski, M. Haase, and H. Weller, Nano Lett. **1**, 207 (2001).
[21] P. Alexandridis and T. J. Mountziaris, U.S. Patent No. 20050006800.
[22] A. H. Nethercot, Phys. Rev. Lett. **33**, 1088 (1974).
[23] M. A. Hines and P. Guyot-Sionnest, J. Phys. Chem. B **102**, 3655 (1998).
[24] X. G. Peng, J. Wickham, and A. P. Alivisatos, J. Am. Chem. Soc. **120**, 5343 (1998).
[25] V. V. Nikesh, A. D. Lad, S. Kimura, S. Nozaki, and S. Mahamuni, J. Appl. Phys. **100**, 113520 (2006).
[26] B. D. Cullity and S. R. Stock, *Elements of X-Ray Diffraction* (Prentice-Hall, New Jersey, 2001), p. 170.
[27] D. J. Norris and M. G. Bawendi, Phys. Rev. B **53**, 16338 (1996).
[28] J. Nanda and D. D. Sarma, J. Appl. Phys. **90**, 2504 (2001).
[29] S. Sapra and D. D. Sarma, Phys. Rev. B **69**, 125304 (2004).
[30] A. V. Nurmikko and R. L. Gunshore, J. Lumin. **52**, 89 (1992).
[31] J.-B. Xia, Phys. Rev. B **40**, 8500 (1989).
[32] Al. L. Efros and M. Rosen, Annu. Rev. Mater. Sci. **30**, 475 (2000).
[33] I. L. Kuskovsky, W. MacDonald, A. O. Govorov, L. Mourokh, X. Wei, M. C. Tamargo, M. Tadic, and F. M. Peeters, Phys. Rev. B **76**, 035342 (2007).
[34] T. Richard, P. Lefebvre, H. Mathieu, and J. Allegre, Phys. Rev. B **53**, 7287 (1996).